Insights into Montmorillonite Nanoclay Based ex Situ Nanocomposites from SEBS and Modified SEBS by Small-Angle X-ray Scattering and Modulated DSC Studies

Anirban Ganguly and Anil K. Bhowmick*

Rubber Technology Center, Indian Institute of Technology, Kharagpur, 721 302, India

Yongjin Li

Nanotechnology Research Institute, National Institute of Advanced Industrial Science and Technology (AIST), Ibaraki, 305-8568, Japan

Received February 6, 2008; Revised Manuscript Received June 16, 2008

ABSTRACT: The work reported here is concerned with the quantification and correlation drawn on the effect of nanoclay platelets in the lamella orders in the nanocomposites of poly[styrene-*b*-(ethylene-*co*-butylene)-*b*-styrene] triblock copolymer (SEBS) and polar-modified SEBSs by using small-angle X-ray scattering (SAXS) and modulated DSC (MDSC) studies with morphological evidence from atomic force microscopy (AFM) and transmission electron microscopy (TEM). 2−4 wt % organically modified nanoclay OMT loading assists increment in the lamellar orders of the neat SEBS owing to interaction in these hybrid systems indicated by the positive shift in glass transition temperature by DSC. Polar-modified SEBS samples show deviation of the corresponding ordering lengths and pattern supported by MDSC, while their unmodified MT nanoclay based nanocomposites exhibit structural regeneration of ordering pattern and morphology evidenced from AFM and TEM due to nucleating effect of the added nanoclay.

Introduction

Polymer−clay nanocomposite is a class of expanding researched systems in the world under hybrid nanocomposite materials in which at least one dimension of the reinforcing phase is in the order of nanometers in the polymer matrix.[1–3] These polymer−clay nanocomposites possess superior properties to conventional microcomposites due to maximized interfacial adhesion and finely dispersed nanoclays distributed all through the polymer matrix.[1–7] The smectite nanoclays as layered silicates are considered in our present investigation for the preparation of polymer-based nanocomposites because of their suitable charge layer density, 2:1 tetrahedral−octahedral layer structure, accommodation of exchangable interlayer cations due to octahedral substitution of +1 or +2 cations for Al^{3+}, high aspect ratio of platelets, and improvements in the mechanical, barrier, and thermal properties of polymer nanocomposites as observed in our earlier studies.[8–11] Specialty elastomer−clay nanocomposites reported from our laboratory have interesting results due to unique interfacial bonding between nanofillers and polymer matrix, which is a function of the rubber, the solvent used for casting, the nature of clay, and so on.[8–13]

Because of the self-assembling characteristics of the block copolymers (BCP),[14,15] various types of block copolymers have attracted attention as nanoscale materials on their own for their microphase separated morphological phenomena.[16–25] Still, less attention has been paid so far to the development of nanocomposites based on thermoplastics elastomers/block copolymers. The work by Ha et al.[26] describes the PS-functionalized montmorillonite NA+ clay layers into SBS microdomains. Though the work explains well the reason for flipping of BCP layers due to clay layers, it demonstrates inferior mechanical properties on clay loading to poly(styrene-*b*-butadiene-*b*-styrene) (SBS) matrix. Though a few studies are available on poly(styrene-*b*-ethylene-*co*-butylene-*b*-styrene) triblock copolymer (S-EB-S)-clay nanocomposites,[26–28] organically modified costly organoclays are employed for compatibility with hydrophobic polymer. For the nonpolar nature of S-EB-S, workers including the present authors[11,12] have found it very difficult to disperse and exfoliate montmorillonite clays (MT) mostly due to the incompatibility with hydrophilic clay from its tactoid form. The versatility of S-EB-S block copolymer has been significantly improved[13] by grafting polar functional groups like maleic anhydride, acrylic acid, and sulfonic acid. This novel approach of synthesizing grafted SEBS−clay nanocomposite has shown that unmodified clay (MT) can be successfully intercalated and exfoliated by grafted SEBS systems.

Though small-angle X-ray scattering (SAXS) and transmission electron microscopy (TEM) investigations on block copolymers have been routine for the past two decades or so,[14–29] detailed SAXS studies along with DSC and modulated DSC for SEBS− and modified SEBS−clay nanocomposites have not been reported and are helpful in correlating microstructure with properties. The work reported here is concerned with the quantification and correlation drawn on the effect of nanoclay platelets in the lamella orders in the nanocomposites of SEBS and modified SEBSs by using SAXS, MDSC studies, and morphologies evidence from atomic force microscopy and transmission electron microscopy.

Experimental Section

Materials and Sample Preparation. The SEBS block copolymer (Kraton G 1652, molecular weight of 57 000) used was obtained from Shell Chemical Co. Ltd., Washington Blvd., OH, and the weight ratio of styrene:ethylene−butylene was 30:70. Grafting reactions, leading to chemical modification of SEBS to impart polarity using maleic anhydride, acrylic acid, and sulfonic acid, were reported in our earlier communication.[13] Unmodified sodium montmorillonite clay (MT, *d*-spacing of 001 plane was 1.17 nm from wide-angle X-ray diffraction) and long-chain quaternary ammonium ion modified nanoclay (OMT, Cloisite20A, *d*-spacing of 001 plane was 2.32 nm from wide-angle X-ray diffraction) were generously supplied by Southern Clay Products, Gonzales, TX. We

* Corresponding author. Phone: (91-3222) 283180. Fax: (91-3222)-220312. E-mail: anilkb@rtc.iitkgp.ernet.in.

10.1021/ma800274y CCC: $40.75
Published on Web 07/22/2008

had adopted a solution intercalation process for dispersing the nanoclays adequately into different SEBS matrices, details of which were discussed in our earlier work.[11–13] Toluene, nonselective to both the phases, was chosen as solvent for synthesis of the nanocomposites. As sulfonated SEBS did not dissolve properly in toluene, we had to go for an appropriate solvent like tetrahydrofuran (THF)/methanol 90:10 mixture. The solution intercalation method was adopted to disperse nanoclays in 10% w/v SEBS solutions with varying clay loading (2, 4, 6, and 8 phw; pbw = parts per 100 parts of SEBS by weight). All the processes were carried out at room temperature, and care was taken to dry off the entire solvent from the samples.

Small-Angle X-ray Scattering Studies. Small-angle X-ray scattering (SAXS) patterns were obtained using microfocused Cu Kα radiation (45 kV, 60 mA) generated by an X-ray diffractometer (Rigaku Ultrax 4153A 172B) and an imaging plate detector at room temperature. The camera length of the SAXS was kept at 740 mm.The exposure time was 4 h for each measurement. Finally, Lorentz correction[30] was performed for all the SAXS profiles, after subtracting the air scattering. The corresponding length (L) of each scattering peak in the profile was calculated following eqs 1 and 2.

$$L = 2\pi/q \tag{1}$$

where q denotes the magnitude of the scattering vector as defined by

$$q = 4\pi\lambda^{-1}\sin(\theta/2) \tag{2}$$

with λ and θ being the wavelength of the incident X-ray beam (λ = 0.154 nm) and the Bragg scattering angle, respectively.

DSC and Modulated DSC. Differential scanning calorimetry (DSC) and modulated DSC (MDSC) studies were carried out in a Q1000 machine by TA Instruments (USA) at a rate of 5 °C/min in an inert atmosphere (N_2 atmosphere) using aluminum pans. The temperature range for DSC studies was from −100 to 150 °C.

The MDSC experiment was conducted at the same range as in DSC for three representative samples and then from 50 to 250 °C for all samples with an additional sinusoidal heating rate (i.e., modulated) of ±0.5 °C every 40 s to improve resolution and sensitivity. Reversible heat flow was correlated with specific heat component and nonreversible with the kinetic component[31–33] as per eq 3.

$$P = C_p\mathrm{d}T/\mathrm{d}t + f(t, T) \tag{3}$$

where T stands for temperature and t for time.

Baseline and temperature calibrations were done in the required temperature range as per ASTM E967 and E968. The total heat flow was segregated into reversible and nonreversible heat flow.[30,31] Modulated DSC is an enhancement to conventional DSC that provides superior sensitivity and accuracy for measurement of reversible and nonreversible heat flows, which is not possible with conventional DSC studies.

Morphology by AFM and TEM. *Atomic Force Microscopy (AFM).* AFM phase images were acquired in tapping mode (TMAFM) using etched silicon probe tips (TESP) in air at ambient conditions (25 °C, 60% RH) using a multimode atomic force microscope from Digital Instruments Inc. (Veeco Metrology Group), Santa Barbara, CA,[34] attached with a Nanoscope IIIa feedback controller. Nominal spring constant of ~40 N m^{-1} and higher length of 225 μm of TESP ensured proper scanning of intricate hard and soft segments in the block copolymer nanocomposites in the present study. Images were recorded with the set point ratio ($r_{sp} = A_{sp}/A_0$, where A_0 = free oscillation amplitude and A_{sp} = set point amplitude selected for the measurement, where the feedback mechanism in TMAFM was controlled by this set point ratio) of 0.8−0.9. In order to have a very smooth surface for AFM analysis, the samples were first cooled to −80 °C by using liquid nitrogen and then sliced by using a diamond knife attached to a Leica Ultracut UCT cryomicrotome unit.

Transmission Electron Microscopy (TEM). Bulk morphology was studied with a JEOL 2010 (Japan) TEM operating at an acceleration voltage of 120 keV in the bright field mode. The approximately 50 nm thick sections required for TEM studies were microtomed at −100 °C using a ultracryomicrotomy using a Leica Ultracut UCT (Vienna, Austria) with a freshly prepared glass knife of cutting edge 45°. These sections were then vapor stained with RuO_4 (ruthenium tetroxide) for $^1/_2$ min at room temperature to differentiate different constituting components in the nanocomposites.[35,36] Digital images of transmission electron micrographs were acquired with a Gatan camera coupled with acquisition.

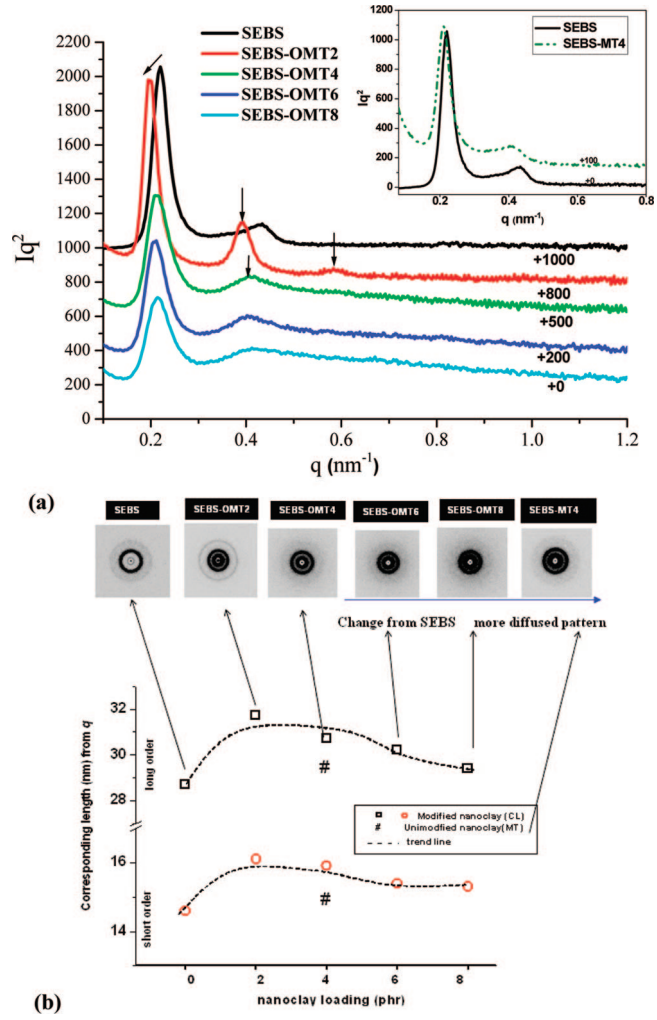

Figure 1. Effect of montmorillonite nanoclay loading on neat SEBS: (a) Lorentz-corrected SAXS profiles (vertically shifted for better clarity) showing effect of nanoclay and (b) lengths corresponding to first- and second-order scattering vector position along with their 2-dimensional SAXS patterns for each sample (indicated at arrowhead) for clay-loaded nanocomposites. (CL = OMT nanoclay).

Results and Discussion

SAXS Studies. The effects of nanoclay on the order structure of SEBS have been evaluated by comparing the intensity vs scattering vector plots by small-angle X-ray scattering (SAXS) for neat SEBS and its nanocomposites (Figure 1a). All the samples show at least two-order scatterings with the peak position ratio of 1:2, indicating the layered (lamellar) structures (Figure 1a). Both the first- and the second-order peaks display a trend of increasing the corresponding lengths calculated from scattering vector positions (q, nm^{-1}) from eqs 1 and 2 with nanoclay loading, among which incorporation of 2 pbw (parts per 100 parts per rubber by weight, here SEBS) loading of organoclay (OMT) has shown the maximum increase with 4 pbw almost having similar effect as shown in the Lorentz-

corrected SAXS profiles in Figure 1a,b. In order to further confirm the effects of nanoclays on SEBS, 2-dimensional SAXS studies were performed, which clearly detect a distinct pattern at 2 pbw of OMT loading. Isotropic circular rings are observed in the 2-D SAXS pattern for the as-cast sample films. These rings are ascribed to diffraction resulting from one-dimensionally alternating lamellar microdomains, and the ratio of q values for the first and second diffraction rings can relatively be assigned to 1:2. After 4 pbw loading of OMT organoclay, the patterns become more and more diffused and corroborate well with SAXS profile. With higher loading of nanoclay, the lamellar ordering length tends to get reduced, especially at 8 pbw loading. The intensity of both the scattering peaks is also found to increase due to good dispersion of clay platelets in SEBS chains for SEBS-OMT2 and SEBS-OMT4 nanocomposites. The ordered structure of SEBS base matrix is maintained with nanoclay loading up to 6 pbw. With 2 pbw of nanoclay loading, the ordering is found to enhance to 1:2:3 as shown in Figure 1a, while SEBS-OMT8 shows a tendency toward lowering of both the scattering peaks and widening of the peaks with scattering peak position disturbed to 1:2.3 in place of exactly 1:2 for neat SEBS. The maximum increase of the corresponding order length is found with only 2 pbw of clay, indicating extensive interaction and excellent dispersion of fine nanometer-sized clay platelets with SEBS chains. The first peak position shifts from $q^* = 0.220$ nm^{-1} (corresponding to the length of 28.5 nm) to $q^* = 0.198$ nm^{-1} (length of 31.7 nm) for this 2 pbw OMT-loaded SEBS-OMT2 nanocomposite, indicating good dispersion and interaction in the matrix. Earlier, the nanocomposites at 2 and 4 pbw of OMT had shown exfoliated morphology (from wide-angle X-ray diffraction) in SEBS.[11,12] The shorter period is also changed on OMT loading. But the unique phase separation really gets disturbed on adding 6−8 pbw of OMT as shown by the diminishing tendency of the second scattering peak. The occurrence of smaller long period of SEBS block copolymers at higher OMT loading indicates that OMT and SEBS have limited compatibility, which yields diffused scattering pattern. This is a result from both enthalpic and entropic interaction between OMT and SEBS. The present SAXS studies on interaction of clay platelets have agreement with the earlier studies.[11−13] This interaction can be correlated with modulated DSC data discussed later.

For nanocomposites with nanoparticle dispersed in a polymer matrix, the SAXS measurements sometimes give a clear form factor scattering peak. This form factor shows the relation with the q of q^{-2}, q^{-3}, or q^{-4} depending upon the shape of the particle and the extent of dispersion of the particles. However, this kind of form factor scattering is seldom found in the polymer composites by melt blending or solvent casting due to the irregular dispersion of the nanoparticles. It can be observed in some gel nanocomposite systems.[37] However, it cannot be confirmed from the present results whether the form factor peaks, if any, is merged with the first or the second scattering peak. Monotonic increment in second ordering peak intensity from neat SEBS to 8 pbw loaded SEBS-OMT8 composite may indicate the presence of this form factor at this region.

For the lamellar structure of SEBS, the peak position (q) of the second-order peak is 2 times of the first peak, indicating the microphase-separated lamellar structure for SEBS in both neat SEBS and nanocomposites.

Similar to the previous analysis, both the neat SEBS and the SEBS-MT nanocomposites have lamellar structure. The periods in SEBS are almost unchanged upon adding MT, inferring insignificant effect of MT clay on SEBS matrix, as shown by the SAXS profile. This is evident from the second ordering peak in Figure 1a (inset) and diffused 2-D pattern in Figure 1b. A similar observation is made from WAXS studies.[11,12]

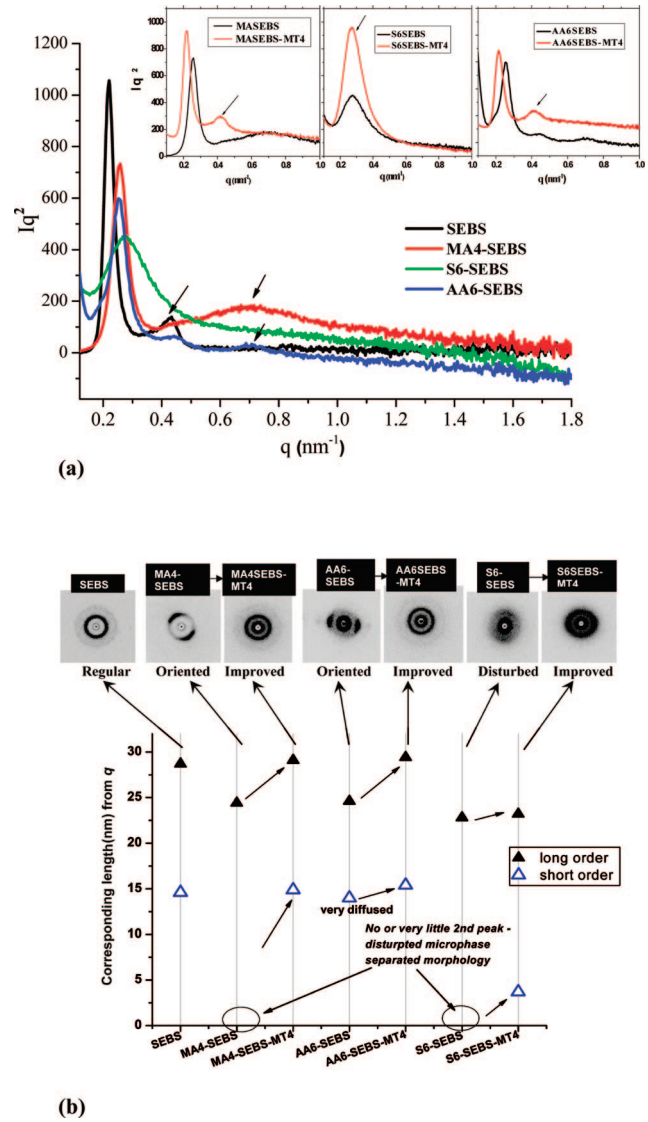

Figure 2. Effect of chemical modification of SEBS: (a) Lorentz-corrected SAXS profiles (insets show MT-based nanocomposites from modified SEBSs); (b) corresponding lengths from first and second ordering scattering vector position along with their 2-dimensional SAXS patterns for each sample (indicated at arrowhead) of modified SEBSs and their corresponding MT4 based nanocomposites.

Chemical modification has clear effect on SEBS microstructure as well-ordered lamellar patterns get disturbed indicated in first and second ordering peaks (Figure 2a,b). The corresponding 2-D SAXS patterns also get diffused and oriented on chemical modification of SEBS as modification brings about changes in the microphase separated ordered morphology. For MA4SEBS (SEBS grafted with 4 wt % maleic anhydride) and AA6SEBS (SEBS grafted with 6 wt % acrylic acid) samples, it is observed that lamellar structure has been retained, but the corresponding order length from first scattering peak becomes smaller compared to SEBS. The ordering pattern also gets disturbed from 1:2 for neat SEBS to 1:7/2 for MA4SEBS and 1:5/2:7/2 for AA6SEBS. Though the later shows a proof of improvement in ordering due to the presence of the third ordering peak, the intensity falls in a very low range. For S6SEBS, the presence of only one distinct but very broad scattering peak indicates distortion of phase-separated morphology and architecture in this case. The difference in the SAXS results between the SEBS and the modified SEBS may be attributed to polarity of the structure, which causes difference in internal phase separation from that of neat SEBS.

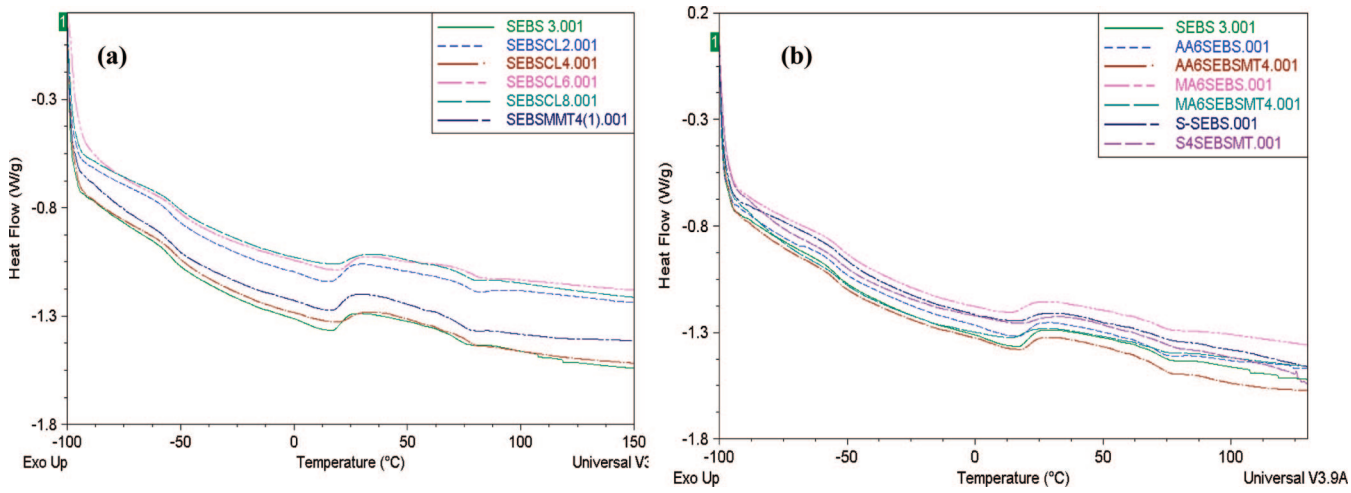

Figure 3. Effect of (a) modified (OMT) and unmodified (MT) clay loading and (b) polar modification and its MT4-based nanocomposites on shift of T_gs from normal DSC traces (CL = OMT nanoclay).

The corresponding order length from first peak for SEBS (denoted by filled symbols in Figure 2b) has clearly decreased on polar modification. On loading 4 pbw of unmodified nanoclay, unlike the previous analysis on neat SEBS and MT clay, this corresponding length has increased from that of the aforesaid modified SEBS polymers, suggesting significant interaction between MT nanoclay and polar-modified polymer chains, thus improving the basic lamellar structure (Figure 2a,b). An important observation is that the ordering pattern has also improved to a peak position ratio of 1:2 for both MA4SEBS-MT4 and AA6SEBS-MT4 nanocomposites. Superlative interaction of MT clay with these polar-grafted SEBS matrices as discussed in our earlier paper explains the results.[11–13] Interfacial tension calculated by the same authors has much lower values (0.03 to 0.6 mJ m^{-2}) for polar-grafted SEBS-MT4 nanocomposites compared to neat SEBS-MT4 composite (1.46 mJ m^{-2}), which explains the easier formation of nanocomposites with MT clays in the former case.

No or very little second peak is seen in Figure 2a due to disturbed phase-separated morphology in the case of the modified SEBS, i.e., MA4SEBS, AA6SEBS, and S6SEBS. This is the reason for getting diffused and oriented 2-D SAXS patterns (Figure 2b) for the modified SEBS systems. Now, the second ordering peak gets regenerated (denoted by open symbols in Figure 2b) on incorporation of 4 wt % of MT nanoclay to these polar-modified SEBS matrices in the resulting nanocomposites, which is also indicated by 2-D SAXS circular patterns for these modified SEBS-MT4 clay nanocomposites. This interesting finding can be observed mainly due to nucleating effect of fine clay layers with a large number of interacting hydroxyl groups in the matrices.

The calculated enlarged corresponding length due to impregnation of MT clay to MA4SEBS matrix has clear effect on order and microphase-separated morphology. Physical properties and wide-angle X-ray diffraction and TEM morphology studies in our earlier publications[11–13] reveal that fine clay layers are fully distributed in MA4SEBS and AA6SEBS matrices in the resulting nanocomposites. Because of the fine lamina of nanoclay layers interacting well with the matrix and acting as nucleating agent, the ordering might have improved for MA4SEBS and AA6SEBS. On sulfonation, the microphase separated morphology gets a distorted form (Figure 2a) in S6SEBS. Addition of MT clay seems to have very little effect on the ordering profile of S6SEBS excepting increasing the order intensity, but the 2-D SAXS pattern suggests regeneration of order structure observed with 4 wt % of MT clay in the nanocomposite.

DSC for T_g Shift. DSC scans of various SEBS samples are shown in Figure 3a,b.

Rubbery block (PEB) T_g at −57 °C for neat SEBS has been shifted to −54 and −53 °C for SEBS-OMT2 and SEBS-OMT4 nanocomposites, respectively, inferring positive interaction between clay and SEBS. This positive shift remains unchanged on further loading of organically modified nanoclay (OMT 6−8 pbw), as the strength of interaction between OMT and SEBS should be characteristics of surface chemistry of OMT and SEBS or on addition of unmodified nanoclay (MT 4 pbw), indicating insignificant interaction. The same trend is observed in the case of plastic (PS) T_g of SEBS with 2−4 pbw OMT-loaded samples showing maximum shift in T_g (from 70 °C for neat SEBS to 77 and 80 °C for SEBS-OMT2 and SEBS-OMT4 nanocomposites, respectively) as shown in thermograms in Figure 3a. MT4-based nanocomposites of AA6SEBS and MA4SEBS register similar positive shift of ∼2−3 °C from their precursor modified SEBS, respectively. T_g for the rubbery PEB segment does not change at all on sulfonating SEBS, while tan δ maxima of PS moiety lowers down and shifts toward positive temperature (72 °C), indicating clear proof that sulfonation reaction has taken place in the styrene moiety only (Figure 3b). In the case of MT4 clay modified SSEBS sample, the T_g for PS further gets shifted to 77 °C, showing considerable interaction between MT clay layers with S-SEBS matrix.

MDSC for Different SEBS Samples. In order to further study these effects of clay loading and modification on SEBS, modulated DSC was carried out. Our work claims to be the first study on SEBS and modified SEBS clay based nanocomposites employing MDSC. In this temperature-modulated DSC, the signals have been divided into two parts: (i) signal dependent on the rate of temperature change connected mainly with the heat capacity of the sample and (ii) signal dependent on the absolute value of temperature connected mainly with the kinetics of physical and chemical transformations as per eq 3.

Total heat flow MDSC traces of representative SEBS, MA6SEBS, and SEBS-OMT samples, as shown in Figure 4a, demonstrate two T_gs for two blocks (rubbery PEB and plastic PS) present in neat, polar-modified and nanocomposite samples (like DSC traces in Figure 3a,b). Apart from two glass transitions for rubbery PEB and plastics PS blocks, one transition near 20 °C occurs (evident in all DSC thermograms in Figure 3a,b and MDSC full scan in Figure 4a) due to the melting of the ordered $-(CH_2-CH_2)_n$ in the poly(ethylene-*co*-1-butene) block (PEB) in SEBS, modified SEBS, and their clay-based nanocomposites. Slight shift is observed in clay-based nanocomposites and also

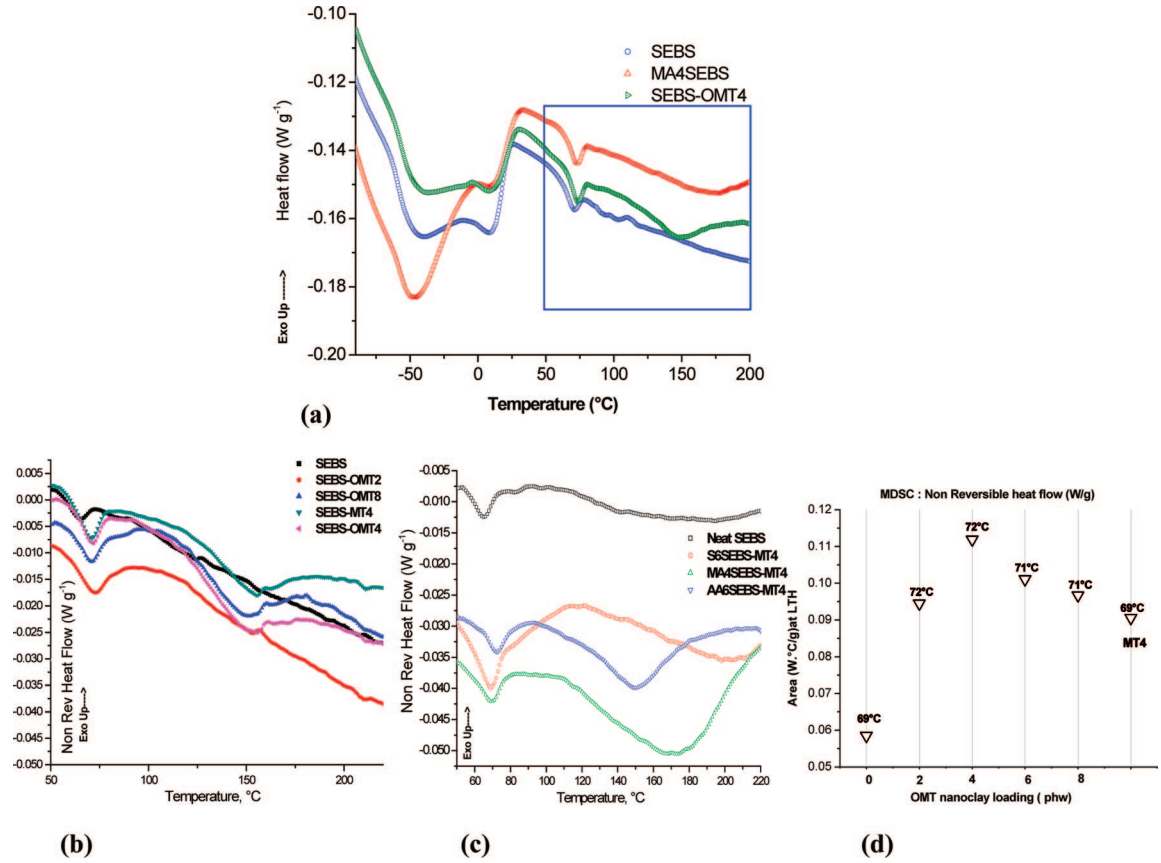

Figure 4. MDSC thermograms for (a) total heat flow of SEBS, MASEBS and SEBS-OMT; nonreversible heat flow for (b) neat SEBS and nanoclay-loaded SEBS nanocomposites and (c) chemically modified SEBS−clay nanocomposites. (d) Analysis of MDSC nonreversible endothermic hump area with corresponding temperature involved in different clay loading on neat SEBS and nanocomposite system.

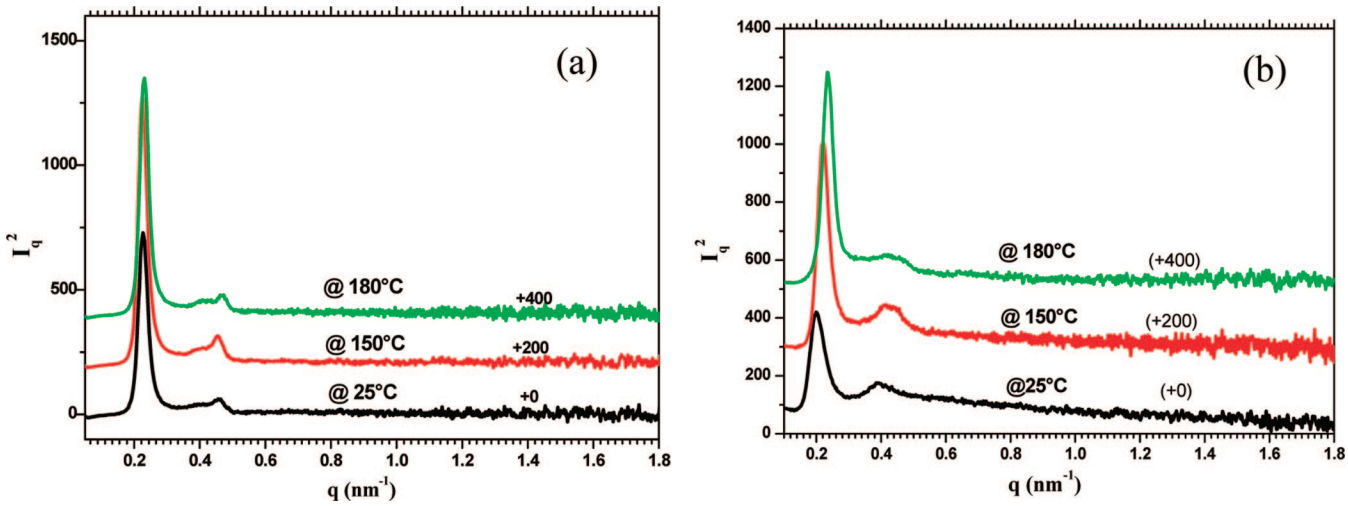

Figure 5. SAXS profiles for (a) neat SEBS and (b) SEBS-OMT4 at room temperature (25 °C), 150, and 180 °C.

in chemically modified SEBS and their nanocomposites (Figure 3a,b and Figure 4a).

These MDSC traces also indicate advent of two endothermic humps at ∼70 °C and ∼150 °C. So, a thorough study by nonreversible MDSC heat flow was carried out on the said range of temperatures (from 50 to 240 °C, indicated by the box in Figure 4a) to investigate further into the behavior of these two humps on clay loading and modification and subsequent nanocomposite preparation (Figure 4b,c). After the T_g of PS moiety of SEBS at ∼69 °C, segmental motion gives rise to an extra endothermic hump at relatively lower temperature (we have termed it as lower temperature hump, LTH). This hump originates due to nonreversible relaxation by partial chain movement. The enthalpy relaxation of PS blocks of SEBS is induced by the framework movement of the side benzene ring and the initiation of softening of the PS phase at this temperature. Now the hump area is increased on increasing the clay or changing the type of clay or modifying the SEBS matrix itself (Figure 4b,c). As the organic surfactant content is very low (clay dose itself is only 2−8 wt %), we can assume that the surfactant plays insignificant role compared to the main SEBS matrix behavior. Another hump originates mostly due to clay−polymer interaction and also for polar-modified samples due to entire movement of PS moiety in the microstructure at

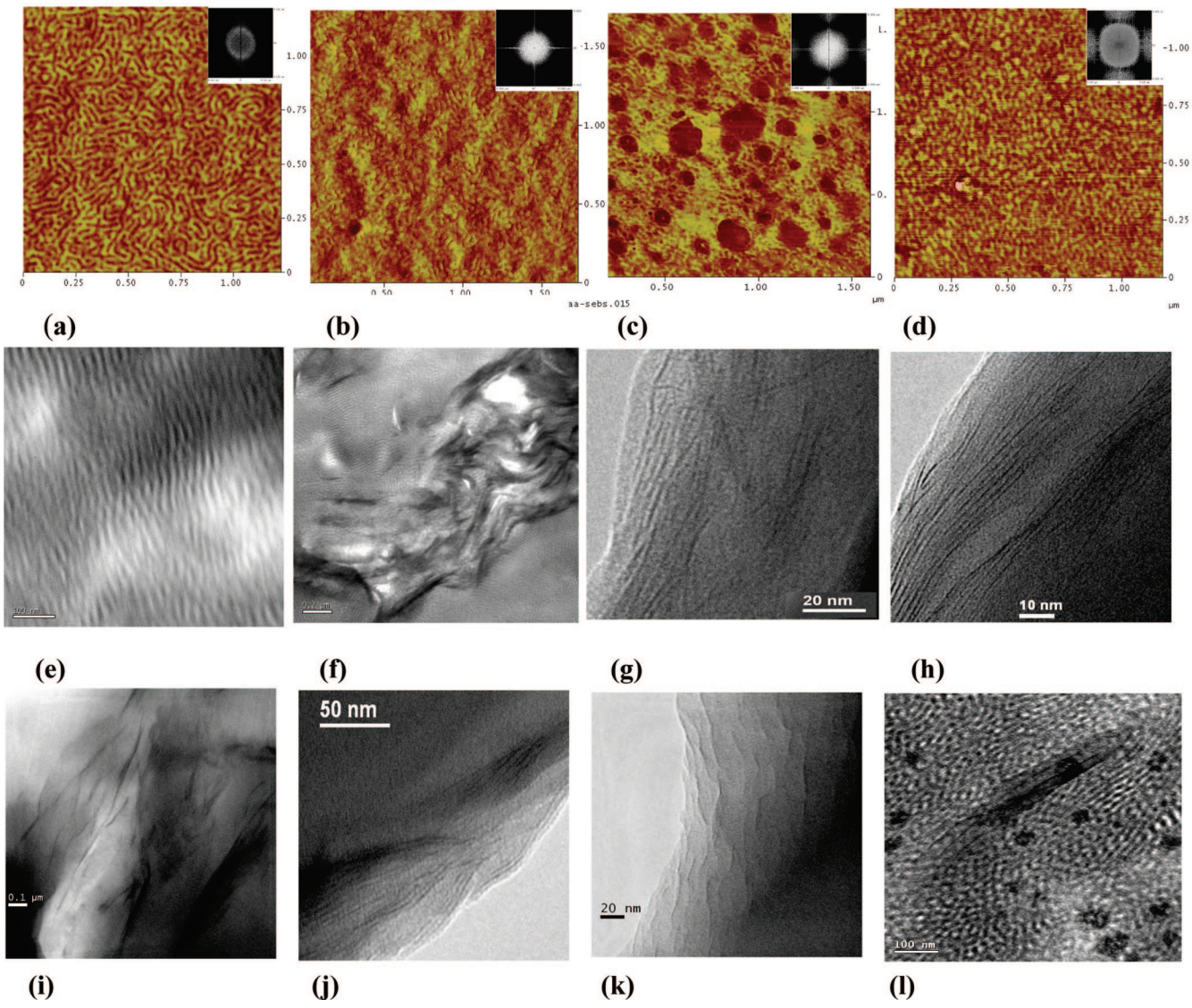

Figure 6. Tapping mode AFM phase images of (a) lamellar spaghetti-like morphology for neat SEBS, (b) oriented morphology of MA4SEBS, (c) lamellar with spherical PEB patchy domains morphology of AA6SEBS, (d) distorted (from lamellar) with near spherical morphology of S6SEBS (all insets show corresponding 2-D FFT). Bright-field TEM morphology of (e) neat SEBS (stained), (f) agglomerated SEBS-MT4 (stained), (g) exfoliated SEBS-OMT2, (h) intercalated−exfoliated SEMS-OMT4, (i) thick stacks of SEBS-OMT8, (j) near−exfoliated MASEBS-MT4, (k) exfoliated SSEBS-MT4, and (l) AA6SEBS-MT4 nanocomposites after selective staining.

∼130−150 °C (higher temperature hump, HTH). This corresponds to the entirely viscous flow temperature of the chains of the PS phase. This is also corroborated from the SAXS studies at high temperature, as discussed later. This type of specific transition has been reported by other workers too in block copolymers.[15–17,19–21] T_g shift as well as area change in these humps can be correlated to interaction of clay platelets with SEBS chains. These nonreversible MDSC thermograms for representative chemically modified SEBS-MT4 nanocomposites (Figure 4c) show much change in irreversible heat flow involved due to interaction between clay and polymer chains.

On adding OMT nanoclay, this hump area (LTH) increases due to irreversible enthalpy relaxation near T_g of PS of SEBS (Figure 4d). Positive shifts of 4−8 °C are also observed on OMT clay filled nanocomposites with a maximum hump area change for SEBS-OMT4 nanocomposite (Figure 4b,d) suggesting maximum interaction and dispersion in this system as corroborated from our SAXS studies. A minimum area change for SEBS-MT4 tally with SAXS results in the previous section. The peak areas have increased much with 2−4 pbw clay loadings. The area gets reduced for 6−8 pbw OMT and 4 pbw of MT loaded nanocomposites from neat SEBS. The above results suggest more unrecoverable energy involved due to interaction of clay and SEBS chains during chain relaxations.

The transition in the form of endothermic hump at ∼150 °C (HTH) arises due to entire movement of PS moiety in SEBS, SEBS-clay and modified SEBSs, as evident from Figure 4a,c. Similar to LTH, the change in area of hump is associated with positive temperature shift. This corroborates nanoscale interaction between nanoclays and the nanodimensioned modified SEBS domains (Figure 4b,d).

At first sight, it was thought that this peak at ∼150 °C arises due to order−order transition. There are a few reports on order−order transition for SEBS in the literature.[19,28,38] In order to verify if order−order transition really occurs in our systems, we carried out high-temperature SAXS for neat SEBS and its nanocomposite (SEBS-OMT4). Almost no change is observed from the SAXS profiles at 150 °C, for both neat SEBS and its nanocomposite (Figure 5a,b). Hence, this transition corresponds to the entirely viscous flow of the fundamental chains of the PS phase.

With polar-modified SEBS matrices, lesser LTH area is observed for AA6SEBS and MA4SEBS mostly due to the change in chemical structure of the polymer matrix itself. For, S6SEBS, the LTH is obtained at 102 °C due to change of its microstructure. On incorporation of MT nanoclay, LTH comes to the relatively original position of previously ascribed for phase-separated ordering (~85 °C) which can be correlated to increment in SAXS intensity with regeneration of 2-D SAXS pattern for the said MT-based nanocomposite (Figure 4c). The exfoliation mechanism of clay platelets has been explained in terms of thermodynamic parameters presented elsewhere.[13] It has been shown that interfacial tension of these modified SEBS-MT4 nanocomposites has lower value compared to neat SEBS-MT4 nanocomposite, indicating easier nanocomposite syntheses for the former. These indicate more interaction between fine clay layers and modified SEBS chains leading to restriction in chain movement and thereby reducing the irreversible heat flow. Now, the HTH hump area is increased and position gets shifted to 170 °C for MASEBS-MT4 due to interaction between SEBS and polar MT clay layers. The similar trend is followed in AA6SEBS-MT4 and S6SEBS-MT4 also.

Morphological Proof by AFM and TEM. In order to correlate the microstructure evaluated by SAXS studies, the neat and hybrid block copolymeric SEBS nanocomposites have also been examined by atomic force microscopy (AFM) and transmission electron microscopy (TEM). As these samples are made from nonselective solvent (toluene) cast process, lamellar architecture is formed as shown by periodicities of the architecture of SEBS from 2-dimensional power spectrum (2-D FFT as inset with each AFM phase image). Microphase-separated lamellar morphology driven by chemical incompatibility between the constituting blocks of neat SEBS as revealed from AFM (Figure 6a) and bright field TEM microphotographs (Figure 6e) are observed to change on chemical modification with structural irregularities in the case of MA4SEBS, AA6SEBS, and S6SEBS (Figure 6b−d). The corresponding 2-D FFTs (insets of Figure 6a−d) of the entire image depict deviations from regular ordered lamellar morphology for these different modified SEBS systems. It clearly shows that lamellar morphology of neat SEBS changes to oriented one for MA4SEBS, lamellar, with spherical PEB patchy domain one for AA6SEBS and distorted morphology for S6SEBS which have full agreement with our SAXS studies. Impregnation of the unmodified nanoclay, MT, into neat SEBS (having proper lamellar morphology as seen through TEM image in Figure 6e), form agglomerated thick stacks (20−50 nm thick) of clay layers (Figure 6f) due to low interaction between the two. When the organoclay (OMT) is impregnated, fine exfoliated clay layers and intercalated−exfoliated layers are observed from TEM picture in Figure 6g,h for SEBS-OMT2 and SEBS-OMT4, respectively. This is mainly due to more interaction of SEBS with OMT nanoclay at low loading corroborating our SAXS studies on these systems. Generation of thicker stacked layers of the same OMT nanoclay can be observed in the case of SEBS-OMT8 (Figure 6i) due to higher loading of clay spoiling the intercalated−exfoliated morphology. With the MT nanoclay, polar-modified MA4SEBS and S6SEBS show interacted hybrid nanocomposite having fine dispersed clay layers as shown in Figure 6, j and k, respectively. TEM image of AA6SEBS-MT4 nanocomposite (Figure 6l) indicates that MT nanoclays are dispersed well with lamellar microphase separated morphology which is regained on addition of the MT nanoclay.

Conclusions

The quantification and correlation drawn on the effect of nanoclay platelets in the lamella orders in the nanocomposites of SEBS and polar-modified SEBSs by using SAXS, DSC, and modulated DSC (MDSC) studies with morphological evidence from atomic force microscopy (AFM) and transmission electron microscopy (TEM) have been reported in this paper. SAXS studies show that, on loading of nanoclay, the corresponding lamellar order lengths (from first and second peaks) increased from that of the neat SEBS polymer, suggesting interaction in these hybrid systems. Two and 4 pbw organoclay (OMT) demonstrate maximum interaction and dispersion, while higher loadings (ca. 8 pbw) impart disturbance in ordering period in the matrix due to presence of thick stacks. Polar-modified SEBS samples show deviation of corresponding ordering lengths and nature, while their unmodified MT nanoclay-based nanocomposite exhibit structural regeneration of ordering pattern and morphology due to nucleating effect of added nanoclay. Shift in T_gs determined from DSC for nanoclay-loaded SEBS and modified SEBS samples has agreement with SAXS studies. The low-temperature endothermic hump near 70 °C is generated due to enthalpy relaxation of PS blocks, which is induced by the partial movement of the side benzene ring and the initiation of softening of the PS phase, whereas the high-temperature hump at ~150 °C is the result of the initiation of entire chains' movement of the PS phase. In the resulting nanocomposites, change in area of these endothermic transitions with nanoclay loading is evident with maximum interaction being predicted in the case of 4 pbw. Neat SEBS registers best interaction and dispersion with 2−4 pbw OMT in the nanocomposites, while polar-modified SEBSs show the same with hydrophilic MT clay at 4 pbw loading. Investigation by AFM and TEM provides proofs of morphology generated on nanoclay loading and shift in morphology on chemical modification and subsequent nanocomposite preparation.

Acknowledgment. A.G. acknowledges the scholarship grant in NDF category by AICTE, New Delhi, India.

References and Notes

(1) Pinnavaia, T. J., Beall, G. W., Eds. *Polymer-Clay Nanocomposites*; John Wiley & Sons, Inc.: New York, 2000.
(2) Giannelis, E. P.; Krishnamoorti, R.; Manias, E. *Adv. Polym. Sci.* **1999**, *138*, 108.
(3) Vaia, R. A.; Giannelis, E. P. *Macromolecules* **1998**, *30*, 8000.
(4) Morgan, A. B.; Gilman, J. W. *J. Appl. Polym. Sci.* **2003**, *87*, 1329.
(5) Roy, S. S.; Okamoto, M. *Prog. Polym. Sci.* **2003**, *28*, 1539.
(6) http://www.bccresearch.com/editors/rp-234r.html (accessed on 22nd January, **2007**).
(7) Usuki, A.; Kojima, Y.; Kawasumi, M.; Okada, A.; Fukushima, Y.; Kurauchi, T.; Kamigaito, O. *J. Mater. Res.* **1993**, *8*, 1174.
(8) Sadhu, S.; Bhowmick, A. K. *Rubber Chem. Technol.* **2003**, *76*, 0860.
(9) Sadhu, S.; Bhowmick, A. K. *J. Polym. Sci.: Part B: Polym Phys.* **2004**, *42*, 1573.
(10) Maiti, M.; Bhowmick, A. K. *J. Polym. Sci.: Part B: Polym. Phys.* **2006**, *44*, 162.
(11) Ganguly, A.; DeSarkar, M.; Bhowmick, A. K. *J. Appl. Polym. Sci.* **2006**, *100*, 2040.
(12) Ganguly, A.; DeSarkar, M.; Bhowmick, A. K. *J. Polym. Sci.: Part B Polym. Phys.* **2007**, *45*, 52.
(13) Ganguly, A.; Bhowmick, A. K. Presented at the 172nd ACS Rubber Division Conference and Students' Colloquium, Cincinnati, OH, 10−12 October, **2006**.
(14) Legge, N. R.; Holden, G.; Schroeder, H. E. *Thermoplastic Elastomers: A Comprehensive Review*; Hanser: New York, 1987.
(15) Hamley, I. *The Physics of Block Copolymers*; Oxford University Press: London, 1998.
(16) Ren, J.; Silva, A. S.; Krishnamoorti, R. *Macromolecules* **2000**, *33*, 3739.
(17) Krishnamoorti, R.; Silva, A. S.; Mitchell, C. A. *J. Chem. Phys.* **2001**, *115*, 7175.
(18) Laurer, J. H.; Bukovnik, R.; Spontak, R. J. *Macromolecules* **1996**, *29*, 5760.
(19) Silva, A. S.; Mitchell, C. A.; Tse, M. F.; Wang, H. C.; Krishnamoorti, R. *J. Chem. Phys.* **2001**, *115*, 7166.
(20) Lee, J. Y.; Park, M. S.; Yang, H. C.; Cho, K.; Kim, J. K. *Polymer* **2003**, *44*, 1705.
(21) Mani, S.; Weiss, R. A.; Cantino, M. E.; Khairallah, L. H.; Hahn, S. F.; Williams, C. E.*Eur. Polym. J.* **2006**, *36*, 215.

(22) Mischenko, N.; Reynders, K.; Mortensen, K.; Scherrenberg, R.; Fontaine, F.; Graulus, R.; Reynaers, H. *Macromolecules* **1994**, *27*, 2345.
(23) Hasimoto, H.; Fujiyama, M.; Hasimoto, T.; Kawai, H. *Macromolecules* **1981**, *14*, 844.
(24) Van Dijk, M. A.; van den Berg, R. *Macromolecules* **1995**, *28*, 6773.
(25) Heck, B.; Arends, P.; Ganter, M.; Kressler, J.; Stühn, B. *Macromolecules* **1997**, *30*, 4559.
(26) Ha, Y. H.; Kwon, Y.; Breiner, T.; Chan, E. P.; Tzianetopoulous, T.; Cohen, R. E.; Boyce, M. C.; Thomas, E. L. *Macromolecules* **2005**, *38*, 2170.
(27) Hasegawa, N.; Usuki, A. *Polym. Bull.* **2003**, *51*, 77.
(28) Lim, S. T.; Lee, C. H.; Kwon, Y. K.; Choi, H. J. *J. Macromol. Sci. Part B: Phys.* **2004**, *43*, 577.
(29) Glatter, O.; Kratky; O. *Small Angle X-ray Scattering*; Academic Press: London, 1982.
(30) Cser, F. J. *Appl. Polym. Sci.* **2001**, *80*, 2300.
(31) Reading, M. *Trends Polym. Sci.* **1993**, *1*, 248.
(32) Reading, M.; Luget, A.; Wilson, R. *Thermochim. Acta* **1994**, *238*, 295.
(33) Ozawa, T.; Katsuhiko, K. *Thermochim. Acta* **1995**, *253*, 183.
(34) *Reference Manual on STM*; Veeco Metrology Group: Santa Barbara, CA, 2003.
(35) Hermel, T. J.; Wu, L.; Hahn, S. F.; Chaffin, K. A.; Gerberich, W. W.; Bates, F. S. *Macromolecules* **2003**, *36*, 2190.
(36) Trent, J. S.; Scheinbeim, J. I.; Couchman, P. R. *Macromolecules* **1983**, *16*, 5819.
(37) Theunissen, E.; Overbergh, N.; Reynaers, H.; Antoun, S.; Jeřoměe, R.; Mortensen, K. *Polymer* **2004**, *45*, 1857.
(38) Modi, M. A.; Krishnamoorti, R.; Tse, M. F.; Wang, H. C. *Macromolecules* **1999**, *32*, 4088.

MA800274Y